UNIVERSITEIT
GENT

**biblio.ugent.be**

The UGent Institutional Repository is the electronic archiving and dissemination platform for all UGent research publications. Ghent University has implemented a mandate stipulating that all academic publications of UGent researchers should be deposited and archived in this repository. Except for items where current copyright restrictions apply, these papers are available in Open Access.

This item is the archived peer-reviewed author-version of:

Verification of the accuracy of CFD simulations in small-scale tunnel and atrium fire configurations

Nele Tilley, Pieter Rauwoens, Bart Merci

In: Fire Safety Journal 46, 186–193, 2011.

**To refer to or to cite this work, please use the citation to the published version:**

**Verification of the Accuracy of CFD Simulations in Small-Scale Tunnel and Atrium Fire Configurations.**

Nele Tilley, Pieter Rauwoens and Bart Merci

Ghent University, Department Of Flow, Heat and Combustion Mechanics,

Sint-Pietersnieuwstraat 41, B-9000 Ghent, Belgium

Corr. author: Nele.Tilley@UGent.be, Tel: +32 9 264 32 91, Fax: +32 9 264 35 75

**Abstract**

In preparation for the use of Computational Fluid Dynamics (CFD) simulation results as 'numerical experiments' in fire research, the agreement with experimental data for two different small-scale set-ups is discussed. The first configuration concerns the position of smoke-free height in case of fire with vertical ventilation in an atrium. The second set-up deals with the critical velocity for smoke backlayering in case of fire in a horizontally ventilated tunnel. An N-percent rule is introduced for the determination of the presence of smoke in the simulation results, based on the local temperature rise. The CFD package FDS is used for the numerical simulations. The paper does not scrutinize the detailed accuracy of the results, as this is hardly possible with any state-of-the-art experimental data at hand. Rather, the global accuracy is discussed with current numerical implementation and models in FDS, considering continuous evolution over different version releases with time. The agreement between the experiments and numerical simulations is very promising. Even when quantitative agreement with experimental data is not perfect, the trends are very well reproduced in the simulations. While much additional work is required, both in CFD as in 'real' experiments, the

results are encouraging for the potential of state-of-the-art CFD to be used as numerical experiments.

## 1 Introduction

Fire safety standards for buildings have long time been based on prescriptive rules. However, there is a world wide evolution towards performance-based design, particularly for large, complex buildings. The question can indeed be raised whether current standards still prevail for complex buildings and modern architecture. Supportive insight in the (lack of) fire safety in a design fire scenario can be provided by the application of CFD (Computational Fluid Dynamics), which can be performed for a specific configuration. However, one step beyond is to consider CFD simulations as 'numerical experiments'. Numerical simulations are relatively cheap (at least in comparison to real large-scale experiments). However, a substantial knowledge of the user is required to perform high-quality CFD simulations and careful application is mandatory. The main advantage of numerical simulations is that a significant amount of different parameters can be varied in order to study their effect. As such, this can lead to further development of fire safety standards. It is desirable to exploit this approach in fire safety research. In particular, one research objective is the improvement of calculation methods to determine the required smoke extraction rate to meet fire safety objectives (such as smoke free heights or smoke free zones) in different types of buildings; including atria and large closed car parks.

Obviously, a 'conditio sine qua non' is then that the CFD simulation results are reliable, i.e. of sufficient accuracy in 'blind' circumstances. Therefore, as a first step to show that CFD has the potential to be used as 'numerical experiments', two experimentally studied small-scale test cases are extensively investigated in this article. The first case concerns fires in a small-scale atrium [1]. A fire in a room, adjacent to the atrium, causes a spill plume to rise in the atrium.

The second test case is a small-scale tunnel experiment [2] with forced mechanical ventilation imposed to avoid the smoke backlayering from the fire. Note that the flow is essentially horizontal, in contrast to the atrium configuration.

For the CFD results, the simulation program Fire Dynamics Simulator (FDS, version 5) [3,4], developed by NIST, was used. However, in principle, other CFD packages could have been used as well. Indeed, it would be very valuable to repeat the study with other CFD packages, investigating their model capability, but this is considered beyond the scope of the present paper. The influence on the results of computational mesh and the thermal boundary conditions will be considered. Most importantly, though, it will be illustrated that agreement of simulation results and experimental data is satisfactory for a wide range of tests, which is promising for the use of CFD as 'numerical experiments'.

## 2 Atrium

In this section, the atrium simulations are discussed. In total, 16 simulations have been performed. Four different heat release rates were studied. For each value of heat release rate, four different extraction rates are imposed. First, the set-up of the original experiments is explained. Afterwards, the numerical set-up of the simulations is

discussed. The search for a reliable method to determine the smoke interface height, based on the temperature profile in the atrium, is discussed in a separate section. Finally, the numerical simulation results are presented.

## 2.1 Experimental set-up

In a recently published paper [1], Poreh et al. carried out a series of experiments in a small-scale atrium configuration (Figure 1). Four different total fire heat release rates ($Q_{conv}$) were created in the room adjacent to the atrium. For each heat release rate, different mass flow rates of smoke ($M$) were mechanically extracted at the ceiling of the atrium, corresponding to a certain smoke free height above the spill edge ($z_s$) in the atrium. The depth ($D_b$) and mass flow rate ($M_b$) of the smoke layer, emerging from the adjacent room, were measured.

The room adjacent to the atrium has size 1.25 m x 0.9 m x 0.6 m, and the atrium itself is 2.5 m x 0.9 m x 3.6 m large.

From these experiments, Equation (1) was deduced in [1] to calculate, for a certain heat release rate, the required smoke extraction mass flow rate, in order to maintain a specific smoke free height above the spill edge in the atrium:

$$\frac{M(z)}{Q_{conv}^{1/3}} = C\left(z + z_0\right) \tag{1}$$

$$\text{with } C = 0.3 C_m \rho_0 W^{2/3} \tag{2}$$

$$z_0 = D_b + \frac{M_b}{C Q_{conv}^{1/3}} \tag{3}$$

and $C_m = 0.21$ for adhered spill plumes.

More recent studies of air entrainment in spill plumes in atria include [5,6]. Here, the intention is not to provide new correlations or insights. The only aim is to illustrate the quality of CFD results, in agreement with the experimental data reported in [1].


## 2.2 Numerical set-up

As mentioned in the introduction, FDS, version 5 [3,4] is used for the numerical simulations. The standard Smagorinsky LES turbulence model [7] is incorporated, with Smagorinsky constant $C_s = 0.2$. The Prandtl number has the constant default value 0.7. Cubic cells of size 2.5 cm are used, resulting in a grid of 561 600 cells. A grid refinement study has been performed in the adjacent room to the atrium. In this refinement case, cells of size 1.25 cm edge are used in the adjacent room, whereas the cells in the atrium are still of size 2.5 cm edge. A characteristic length scale of the fire can be calculated as

$$D^* = \left( \frac{Q}{\rho_\infty T_\infty c_p \sqrt{g}} \right)^{2/5} . \tag{4}$$

In the refinement case under consideration, the total fire heat release rate is 8.272 kW, resulting in a dimensionless diameter D* = 0.14 m. As stated in [8], a criterion to guarantee reliable LES-results might be that at least ten cells must fit within the dimensionless diameter. This is satisfied in the refinement case. However, results of this simulation show no difference with the results from the coarser grid simulation. It can therefore be argued that the grid of cell size 2.5 cm is sufficiently fine. Indeed, the detailed configuration of the smoke plume in the adjacent room is of secondary importance with respect to the main smoke field in the large atrium.

In the simulations, radiation is turned off, so that the fire heat release rate corresponds to

$Q_{conv}$. The total heat release rate of the fire can be reconstructed as $Q = Q_{conv} / (1 - \chi_r)$.

This way, uncertainties due to radiation modeling are avoided in the simulations.

All walls are modeled as adiabatic, in agreement with turning off the radiative heat

transfer.

In [1], only values of the convective heat release rate are reported, measured in the

emerging smoke layer underneath the spill edge. Therefore the convective heat release

rate is imposed as fire source in the simulations, with adiabatic walls. The highest

temperatures obviously occur in the adjacent room to the atrium, so that by far most of

the radiative loss would be found there if radiation modeling were included in the

simulations. In the atrium, the plume adheres to the wall. Plume temperatures are

relatively low, so radiative losses are negligible within the atrium itself. However, when

modeling the walls as adiabatic, no heat is lost by conduction through the walls. The

advantage of using non-adiabatic wall conditions would be that convective and

conductive heat transfer could be calculated. Yet, the results discussed below, are hardly

affected by these heat losses (not shown).

It is also important to appreciate that LES are unsteady in nature. Therefore, it is

important to discuss the simulation results in terms of 'averages'.The simulations are

executed until a quasi-steady-state situation is reached. The data between two time

values ($t_1$ and $t_2$) in the quasi-steady state are then time averaged. These averages are

presented below as the 'simulation results'. The times used for averaging the results

depend on the fire heat release rate. Time varies with velocity and length scale as $t \sim L /$

$v$. With Froude scaling, the scaling for velocity is $v \sim Q / L^2$, resulting in scaling of time

with heat release rate:

$$t \sim L^3 / Q. \qquad\qquad (5)$$

With Eq. (5), the averaging period $t_1 - t_2$ is constructed, the values of which are reported in Table 1. These average values are larger than turbulent time scales: from unsteady $k - \varepsilon$ calculations of the same atrium set-up, the turbulent time scale could be calculated as $t_t = k / \varepsilon$ and the maximum value observed was 13 s (not shown).

**2.3 Determination of the smoke layer interface height**

In this CFD study, small-scale atrium experiments are studied, in order to compare the numerical results to the experiments. However, a criterion is first developed to define the height of the smoke layer in the atrium from the simulation results.

The left side of figure 2 depicts a typical temperature profile on a vertical line in the atrium. This profile shows a first (small) increase in temperature at $z = 0.6$ m, i.e. the height of the right-hand side opening (Figure 1). However, this first temperature rise must not be mistaken for the smoke layer interface, as it is not (Figure 2, right). Therefore, the criterion developed to determine the smoke layer interface should take this into account.

Four different methods for the determination of the smoke layer interface are discussed. A first method to determine the interface height of the smoke layer is the equation developed by Thomas et al. [9]:

$$H - z_{\text{int}} = \frac{\int_0^H \dfrac{T - T_0}{T} dz}{\dfrac{T_{av,s} - T_0}{T_{av,s}}}. \qquad\qquad (6)$$

The integration in this formula is performed using the temperatures from the numerical simulations. However, there is a major disadvantage: the equation implies an iterative procedure. Indeed, the smoke layer interface height is on the left hand side of the equation ($z_{int}$), but in order to calculate this, the average temperature of the smoke layer is needed ($T_{av,s}$), which can only be calculated if the interface height is already known. This makes the 'Thomas method' a time consuming procedure.

A second method, described in the FDS user guide [4], relies on a calculation method by He et al. [10]. First, the parameters $I_1$ and $I_2$ are calculated on a vertical line. The temperature $T_l$ is chosen as the lowest temperature on this vertical line. From this, the value of $z_{int}$ can be calculated:

$$I_1 = \int_0^H T dz \text{ and } I_2 = \int_0^H \frac{1}{T} dz \qquad (7)$$

$$z_{\text{int}} = \frac{T_l \left( I_1 I_2 - H^2 \right)}{I_1 + I_2 T_l^2 - 2HT_l} \qquad (8)$$

The third option relies on the second derivative of the temperature profile. Figure 3 reveals that this might indeed be used to indicate the smoke layer interface height. Using a central scheme to calculate this second derivative at height $z = z_k$ (where $k$ is the index of the computational cell in the vertical direction, $z_k = k \, \Delta z$), divided by the local temperature difference:

$$\frac{\partial^2 T}{\partial z^2 \Delta T} \approx \frac{T_{k-1} - 2T_k + T_{k+1}}{\left( \Delta z \right)^2 \left( T_k - T_0 \right)}, \qquad (9)$$

a local maximum of the second derivative can indeed indicate the smoke layer interface (Figure 3, left). However, this is a local maximum. Indeed, at the first temperature rise in the atrium, around $z = 0.6$ m (see Figure 1), a much higher value of second derivative

is found. Therefore, it is up to the user to define whether the local maximum corresponds to the smoke layer interface height, and it requires a visual detection. Thus, the method of the second derivative is not unambiguous and cannot easily be made automatic.

As final method the determination of the smoke layer interface height by the N-percent rule [11] is considered. An interface temperature is then defined by the following formula:

$$T_{\text{int}} = T_0 + \left(T_{\text{max}} - T_0\right)N/100 \qquad (10)$$

In the example of Figure 3, the variation of $z_{int}$ with $N$ is moderate (between 1.3 m and 1.5 m) in the range $10 < N < 65$. The value $N = 30$ is chosen (equivalent to $z_{int} = 1.4$ m in Fig. 3, right). The difference in interface height between elsewhere reported values for $N$ ($N = 10$, 15, 20 [12]) with $N = 30$ is very small in the study under consideration. The main reason for choosing the value $N = 30$ is to avoid that the temperature rise around $z = 0.6$ m be mistaken for the smoke layer interface height in any of the cases. This method is an easily applicable and unambiguous way to determine the smoke layer interface height in the atrium. An important advantage of this method is that it is not time-consuming and can easily be used in the post-processing of simulation data.

Figure 4 displays the smoke layer interface height as obtained with each of the four methods. The results are compared to the height, obtained from Equation 1 with the imposed smoke extraction mass flow rate and fire heat release rate. The first three methods result in an underestimation of the smoke-free height in the atrium compared to the experimental value. The N-percent method, with N = 30, provides a good

approximation of the calculated interface height. This trend was also observed with other fire heat release rate values and smoke extraction flow rates (not shown). Therefore, the N-percentage method is used from now on to determine the smoke layer interface height in the simulations.

## 2.4 Numerical simulation results

Table 2 provides a quantitative overview of the CFD simulation results. In every simulation, the convective heat release rate ($Q_{conv}$) is imposed in the adjacent room, as well as the outlet velocity ($v_{out}$) at the ceiling of the atrium. The other important values of the simulations are then calculated:

- $D_b$, the thickness of the smoke layer emerging from the adjacent room, is calculated with the N-percent method in the plane x = 1.25 m, i.e. the vertical plane of the opening between the room and the atrium (Figure 1).

- $M_b$, the mass flow rate of the emerging smoke layer, is calculated in the same plane as $D_b$. A summation is made over all cells in the plane, only taking into account outflow, $v_{x,n} > 0$, not the inflow of air into the adjacent room:

$$M_b = \sum_n \max\left(\rho_n \cdot v_{x,n} \cdot A_n ; 0\right) \qquad (11)$$

- $M(z)$, the extraction mass flow rate, at the ceiling of the atrium, is calculated in a similar way as $M_b$, considering now only the cells in the outlet opening:

$$M(z) = \sum_n \left(\rho_n \cdot v_{out,n} \cdot A_n\right) \qquad (12)$$

- $z$, the smoke free height above the spill edge in the atrium, is calculated with the N-percent method in the vertical symmetry plane in the atrium (y = 0.45 m).

- $z_0$, the virtual origin, is calculated from the above values with Eq. (3).

Figure 5 depicts these results in a graph. The numerical results (black dots) are in very good agreement with the experimental data (open symbols) and with Eq. 1 (black line). This is very promising for the use of CFD simulations as "numerical experiments".

As using computational codes to solve fire-related problems is still a quite recent research topic, all available CFD-codes are continuously under development. Each new release of a code therefore contains even better algorithms, new developments and extra included options. Care must be taken that simulation results are not very sensitive to the version of the CFD package used. In the process of the research, FDS was upgraded to version 5. Figure 6 shows that differences with results of FDS, version 4, are very small, so that the argument that CFD simulations can be used as "numerical experiments", does not depend on the version used here.

## 3. Tunnel

### 3.1 Introduction

In tunnel configurations with mechanically forced longitudinal ventilation, a key parameter is the critical velocity. This is the minimum velocity required to prevent backlayering in the tunnel, i.e. there is no smoke flow in the opposite direction of the ventilation. The possible hazard of fire spread due to ventilation is not considered here [13].

A paper by Wu and Bakar [2] describes a set of experiments on five small-scale tunnels. Only 'tunnel D', which has a rectangular cross-section, is discussed here. Having the lowest height (0.25 m) to width (1 m) aspect ratio in the series of [2], this tunnel is most similar to a closed car park, a longer term research objective. The Wu and Bakar tunnel

experiments are an extensive study of the variation of critical velocity with heat release rate in tunnels. The low aspect ratio of tunnel D is especially interesting to validate the numerical simulations, for a future study of car parks. The formula for critical velocity that was derived by Wu and Bakar from their experiments is still widely used for tunnel ventilation design.

Other numerical studies have already been reported with validation of the simulations by comparing with the Wu and Bakar experiments (e.g. [14]). Below, the application of the N-percent rule is specifically discussed, as well as the possibility of using adiabatic wall conditions in combination with absence of radiation modeling.


## 3.2 Configuration and set-up

The simulations are performed with FDS, version 5. The tunnel is, as mentioned, 0.25 m (high) by 1 m (wide) by 5 m (long). The computational mesh consists of 640 000 cubic cells of size 1.25 cm.

Two different sets of CFD simulations are performed (73 in total). In the first set, the total (steady) fire heat release rate is imposed and standard FDS radiation modeling and thermal boundary conditions are applied. For radiative heat transfer in FDS, a radiation transport equation for a grey gas is solved. The source term in this transport equation is radiation intensity, described by Planck's law. [3,4] As the radiation intensity defined by Planck's law is highly temperature dependent ($I_b \sim T^4$), small temperature over- or underestimations van lead to large differences in radiation. Therefore, one could consider excluding uncertainties from radiation modeling by only inserting the steady convective heat release rate into the domain. As radiation from the fire mainly heats up the walls, the walls are set to adiabatic in the simulations without radiation. Otherwise,

too much of the (convective) heat from the fire would be used in heating up the walls. This approach is followed in the second set of simulations.

Propane is used as fuel in the simulations, as in the experiments [2].

Again, the standard Smagorinsky model with $C_S = 0.2$ (default in FDS) is used. In [15], it is shown that the influence of the exact value is not large on the results (as long as it does not deviate too strongly from the default value).

A constant velocity is imposed over the entire inlet surface of the tunnel, upstream of the fire.

A quasi steady-state is reached in the simulations after about 120 s for the lowest heat release rate studied. Time-averaged values, determined between 160 s and 180 s, are presented as simulation results for temperature, density and velocity. From previous work [15], a maximum value of turbulent time scale of 5 s was found for $k - \varepsilon$ simulations of the same set-up. Again, the averaging period much larger than the turbulent time scales.

In each simulation, a constant velocity ($v_{in}$) is imposed over the entire inlet area of the tunnel. For each inlet velocity, the corresponding backlayering distance is calculated in the simulations by using the N-percent method (Eq. (10)) on the horizontal centre line at ceiling level (with N = 5). Due to the low value of $N$, a small temperature increase will already result in the detection of the smoke layer at ceiling level, comparable to the use of thermocouples in the original experiments [2]. Extrapolation of these backlayering distances results in the critical velocity, corresponding to a backlayering distance of 0 m for each heat release rate (Figure 7). This method is identical to what is described in [2].

## 3.3 Simulation results

Table 3 lists the experimental data and simulation results for the critical velocity, corresponding to each studied heat release rate with default FDS radiation modeling and thermal boundary conditions. For every heat release rate, the radiative fraction $\chi_r$ as found in the simulations is also listed. This is the fraction of heat loss through radiation to the total heat release rate of the fire:

$$\chi_r = \frac{\dot{Q}_{rad}}{\dot{Q}} \text{ and } \dot{Q} = \dot{Q}_{conv} + \dot{Q}_{cond} + \dot{Q}_{rad}, \qquad (13)$$

with $\dot{Q}$, $\dot{Q}_{conv}$, $\dot{Q}_{cond}$ and $\dot{Q}_{rad}$ the total heat release rate and convective, conductive and radiation heat losses respectively. The radiation heat loss is calculated by integrating the directional radiation intensity over a default number of angles and over the entire domain boundaries [3,4]. In the simulations, the resulting radiative fraction increases with increasing heat release rate from 37% up to 48%.

Table 4 shows the results for the critical velocity in the simulations without radiation losses and with adiabatic walls. The imposed heat release rate in the numerical simulations now corresponds to the convective heat release rate. Estimating the radiative loss fraction at $\chi_r = 0.43$ (Table 3), the corresponding total heat release rate can be calculated.

Figure 8 summarizes the results. The picture reveals two aspects.
Firstly, the simulations with the default settings and the simulations without radiation modeling provide very similar results. This shows that the approach of imposing the convective heat release rate in the numerical simulations, turning off radiation modeling and treating the walls as adiabatic, is valid for the test case under study.

The second observation is that, whereas the trend for the critical ventilation velocity as function of total heat release rate is very well reproduced, the simulation results overestimate the absolute value of the critical velocity, in line with [15], where tunnel B was examined. A difference, defined as the ratio of the deviation between experimental value and simulation value to the experimental value, of about 25% is found between the experimental and numerical results. This deviation might be due to extra water cooling of the tunnel in the neighborhood of the fire in the experimental set-up, as mentioned in [2]: when the tunnel walls reached "high" temperatures, they were cooled with water. As this cooling extracts heat from the tunnel, the experimentally measured critical velocity for a "given" fire heat release rate, in fact corresponds to a lower heat release rate value than what is imposed at the burner. The latter value is applied in the numerical simulations. Unfortunately, no details on the water cooling are provided in [2]. Therefore, the temperatures from the CFD results is used to estimate from what heat release rate value onwards, cooling was applied. Table 5 shows the maximum temperatures $T_{max}$ near the ceiling in the numerical simulations. In the experiments, it can be suspected that as the tunnel walls near the fire are made of stainless steel, cooling was almost certainly applied when the heat release rate exceeded 10.5 kW and perhaps already at 7.5 kW.

The heat loss by cooling is estimated as follows. The steel area of the ceiling of the experimental tunnel set-up is $A_c = 2.4$ m$^2$. The convection coefficient at the inside of the tunnel is estimated as $h = 10$ W/m$^2$K to $h = 15$ W/m$^2$K. Cooling is assumed from the temperatures, obtained in the CFD simulations (i.e. without the water cooling), to 100°C, the boiling temperature for the water at the outside of the tunnel. This implies neglect of thermal resistance caused by conduction in the stainless steel, which indeed

has a high conductivity. The heat, removed per unit time from the configuration by the water cooling, can then be calculated as:

$$Q_{loss} = h \cdot \int_{A_c} \max \left( T - 373; 0 \right) dA \,. \qquad (14)$$

A correction of the experimental heat release rate in this sense clearly brings the experimental results closer to the numerical simulation results. A similar argument was provided in a recently published paper by Li [16], where critical velocities in tunnel experiments are somewhat higher than in the Wu and Bakar tunnel experiments. The corresponding values for this estimated heat loss are listed in Table 5, and indicated with squares in Figure 8.

The observation that the trend of the dependence of the critical velocity on the fire heat release rate is well reproduced in the numerical simulations and that deviations – after the correction as described – are less than 10%, allows to conclude that the simulation results are in satisfactory agreement with experimental data for this tunnel configuration.

## 4. Conclusions

Small-scale experiments of fire in an atrium and a tunnel were repeated as numerical CFD simulations. Both cases concern smoke movement and the formation of a quasi steady-state smoke layer.

Several criteria to define the smoke layer interface were studied, of which the N-percent rule (with N = 30) prevails, as it provides results in good agreement with experiments and it is the most unambiguous method.

For the atrium configuration, very good agreement was found between the experimental and numerical results.

In the tunnel simulations, calculations without radiation modeling and using adiabatic walls proved to be a valid alternative for more time-consuming simulations with radiation modeling. Quite good agreement was found between experimental and numerical results, especially when considering the heat loss due to water cooling in the experiments.

An overall conclusion is that the prediction of the quasi steady-state smoke region by CFD is good, especially when the experiments are well documented. Therefore, it is argued that a parameter variation study with numerical simulations within similar configurations is very useful to obtain qualitative results, a good prediction of the trends and insight into the physics of the configurations at hand.

**References**

[1]     Poreh M., Marshall NR, Regev A., Entrainment by adhered two-dimensional plumes, Fire Safety Journal 2008;43:344-350

[2]     Wu Y, Bakar MZA, Control of smoke flow in tunnel fires using longitudinal ventilation systems – a study of the critical velocity, Fire Safety Journal 2000;35:363-390

[3]     McGrattan K, Hostikka S, Floyd J, Baum H, Rehm R, Mell W, McDermott R, Fire Dynamics Simulator (Version 5) Technical Reference Guide, NIST 1018-5, National Institute of Standards and Technology, 2008

[4]     McGrattan K, Klein B, Hostikka S, Floyd J, Fire Dynamics Simulator (Version 5) User's Guide, NIST 1019-5, National Institute of Standards and Technology, 2008

[5]     Harrison R, Spearpoint M, Physical scale modelling of adhered spill plume entrainment, Fire Safety Journal 2010;45:149-158

[6]     Kumar S, Cox G and Thomas P H, Air entrainment into balcony spill plumes, Fire Safety Journal 2010;45:159-167

[7]     Smagorinsky J, General Circulation Experiments with the Primitive Equations. I. The Basic Experiment, Monthly Weather Review 1963;91:99-164

[8]     McGrattan KB, Baum HR, Rehm RG,Large Eddy Simulations of Smoke Movement, Fire Safety Journal 1998;30:161-178

[9]     Thomas PH, Hinkley PL, Theobald CR, Simms DL, Investigations into the flow of hot gases in roof venting. Fire research technical paper no.7, London: The Stationary Office, 1963

[10]    He Y, Fernando A, Luo M, Determination of interface height from measured parameter profile in enclosure fire experiment, Fire Safety Journal 1998;31:19-39

[11]    Cooper LY, Harkleroad M, Quintiere J, Reinkinen W, An Experimental Study of Upper Hot Layer Stratification in Full-Scale Multiroom Fire Scenarios, Journal of Heat Transfer 1982;104:741-749

[12]    Chow W, Determination of the Smoke Layer Interface Height for Hot Smoke Tests in Big Halls, Journal of Fire Science 2009; 27:125-142

[13]    Beard A, Carvel R, The handbook of tunnel fire safety, Thomas Telford Services Ltd, London, 2005

[14]    Hwang CC, Edwards JC, The critical ventilation velocity in tunnel fires – a computer simulation, Fire Safety Journal 2005;40:213-244

[15]    Van Maele K, Merci B, Application of RANS and LES field simulations to predict the critical ventilation velocity in longitudinally ventilated horizontal tunnels, Fire Safety Journal 2008;43:598-609

[16]    Li YZ, Lei B, Ingason H, Study of critical velocity and backlayering length in longitudinally ventilated tunnel fires, Fire Safety Journal 2010, 45: 361-370
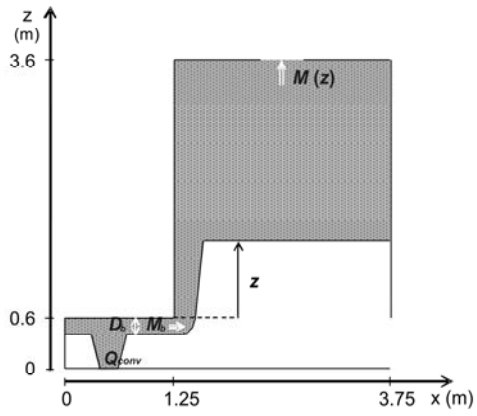
**Figures**
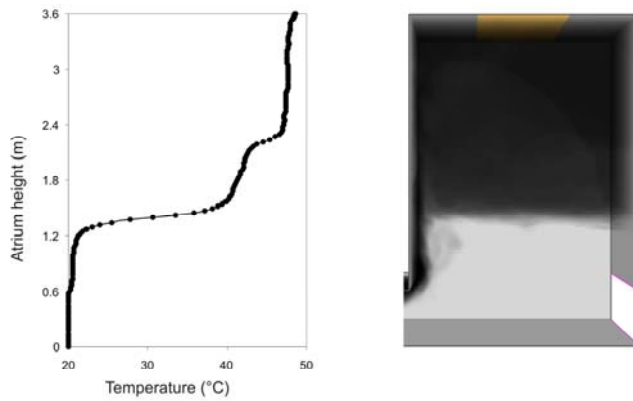


**Figure 1.** Atrium configuration



**Figure 2.** Temperature variation on a vertical line (x = 3.75 m) in the atrium.
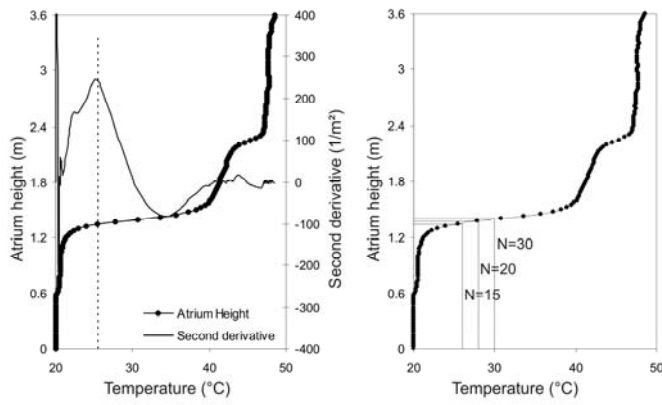
**Figure 3.** Second derivative of temperature in the atrium (left) and N-percent rule in atrium (right).
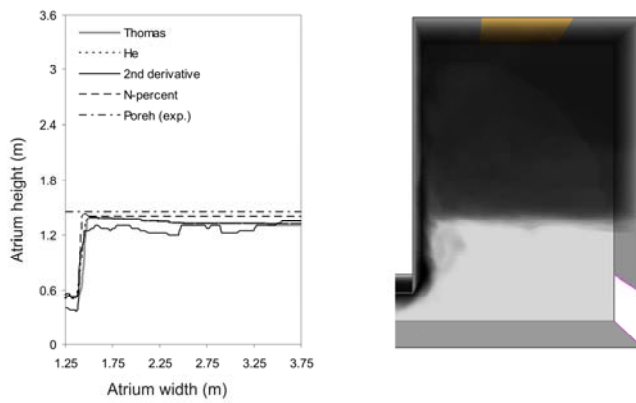


**Figure 4.** Interface height in the atrium.
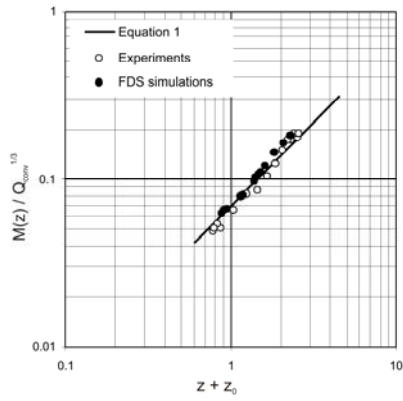
**Figure 5.** Experimental and CFD results of smoke mass flow extraction rate as function of rise height.
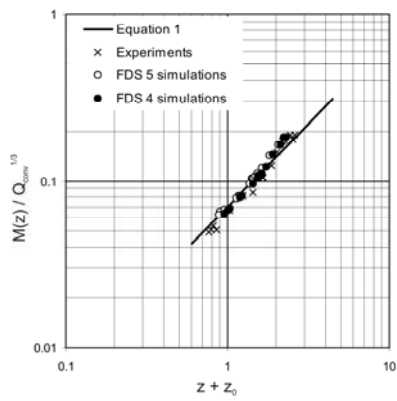


**Figure 6.** Comparison of FDS 4 and FDS 5 numerical results with experiments.

**Figure 7.** Extrapolation to determine critical velocity in tunnel D with heat release rate 12 kW (with standard FDS radiation modeling).
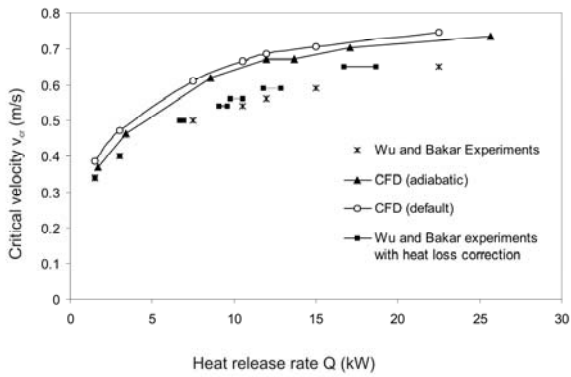


**Figure 8.** Experimental and numerical results for $v_{cr}$ in tunnel D. The squares represent the possible effect of heat loss in the experiments by cooling of the ceiling near the fire.

**Tables**

**List of symbols**

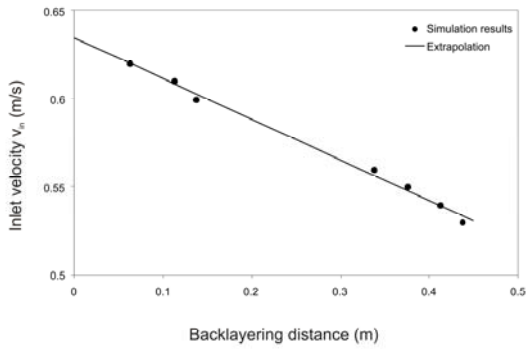| | | |
|---|---|---|
| $A$ | area | $m^2$ |
| $A_c$ | ceiling area | $m^2$ |
| $A_n$ | area of cell n | $m^2$ |
| $C$ | coefficient | $kg/(m.s.kW^{1/3})$ |
| $C_m$ | coefficient | $m^{4/3}/(s.kW^{1/3})$ |
| $c_p$ | heat capacity | J/kg K |
| $C_s$ | Smagorinsky constant | |
| $d$ | backlayering distance | m |
| $D^*$ | characteristic length scale | m |
| $D_b$ | thickness of emerging smoke layer | m |
| $g$ | gravitational acceleration | $m/s^2$ |
| $H$ | total height of atrium | m |
| $h$ | convection coefficient | $W/m^2K$ |
| $I_1$ | parameter | K.m |
| $I_2$ | parameter | m/K |
| $I_b$ | radiation intensity source term | $kW/m^2$ |
| $k$ | cell number | |
| $k$ | turbulent kinetic energy | $m^2/s^2$ |
| $M$ | mass flow rate | kg/s |
| $M_b$ | emerging smoke layer mass flow rate | kg/s |
| $N$ | number in N-percentage rule | |
| $Q$ | total heat release rate of fire | kW |

| | | |
|---|---|---|
| $Q_{cond}$ | conductive heat loss | kW |
| $Q_{conv}$ | convective heat release rate of fire | kW |
| $Q_{loss}$ | heat release rate lost due to cooling | kW |
| $Q_{rad}$ | radiative heat loss | kW |
| $T$ | temperature | K |
| $t$ | time | s |
| $T_{av,s}$ | average smoke layer temperature | K |
| $T_{int}$ | interface temperature of the smoke layer | K |
| $T_k$ | temperature of cell k | K |
| $T_l$ | minimum temperature on vertical line | K |
| $T_{max}$ | maximum temperature | K |
| $T_o$ | ambient temperature | K |
| $t_t$ | turbulent time scale | s |
| $v$ | velocity | m/s |
| $v_{cr}$ | critical velocity | m/s |
| $v_{in}$ | inlet velocity | m/s |
| $v_{out}$ | outlet velocity imposed at ceiling of atrium | m/s |
| $W$ | width of atrium | m |
| $x$ | length | m |
| $z$ | height above spill edge | m |
| $z_0$ | virtual origin height | m |
| $z_{int}$ | interface height of the smoke layer | m |
| $z_k$ | height of cell k above ground | m |
| $\Delta z$ | vertical cell size | m |

| $\chi_r$ | radiative fraction | |
| $\varepsilon$ | turbulent dissipation | $m^2/s^3$ |
| $\rho_o$ | ambient density | $kg/m^3$ |

**Table 1.** Begin ($t_1$) and end ($t_2$) times for the calculation of time-averaged simulation results.

| $Q$ | $t_1$ | $t_2$ |
|---|---|---|
| (kW) | (s) | (s) |
| 4.44 | 261 | 335 |
| 8.27 | 140 | 180 |
| 13.5 | 86 | 110 |
| 18.3 | 63 | 81 |

**Table 2**. Simulation results in the small-scale atrium.

| $Q_{conv}$ | $D_b$ | $M_b$ | $z$ | $M(z)$ | $z_0$ | $z + z_0$ | $M(z)/Q_{conv}^{1/3}$ |
|---|---|---|---|---|---|---|---|
| (kW) | (m) | (kg/s) | (m) | (kg/s) | (m) | (m) | kg/(skW$^{1/3}$) |
| 2.887 | 0.13 | 0.05 | 0.25 | 0.09 | 0.65 | 1.50 | 0.06 |
| 2.887 | 0.13 | 0.05 | 0.53 | 0.12 | 0.65 | 1.78 | 0.08 |
| 2.887 | 0.13 | 0.06 | 0.68 | 0.14 | 0.69 | 1.97 | 0.10 |
| 2.887 | 0.12 | 0.05 | 0.78 | 0.15 | 0.63 | 2.01 | 0.11 |
| 5.377 | 0.13 | 0.07 | 0.28 | 0.12 | 0.68 | 1.55 | 0.07 |
| 5.377 | 0.13 | 0.06 | 0.50 | 0.14 | 0.63 | 1.73 | 0.08 |
| 5.377 | 0.13 | 0.06 | 0.80 | 0.18 | 0.63 | 2.03 | 0.10 |
| 5.377 | 0.13 | 0.06 | 1.00 | 0.21 | 0.62 | 2.22 | 0.12 |
| 8.792 | 0.13 | 0.07 | 0.23 | 0.13 | 0.65 | 1.48 | 0.06 |
| 8.792 | 0.13 | 0.07 | 0.85 | 0.22 | 0.62 | 2.07 | 0.11 |
| 8.792 | 0.13 | 0.07 | 1.19 | 0.30 | 0.63 | 2.42 | 0.15 |
| 8.792 | 0.15 | 0.08 | 1.59 | 0.38 | 0.70 | 2.89 | 0.18 |
| 11.901 | 0.13 | 0.08 | 0.34 | 0.15 | 0.62 | 1.55 | 0.07 |
| 11.901 | 0.13 | 0.08 | 0.90 | 0.25 | 0.62 | 2.12 | 0.11 |
| 11.901 | 0.13 | 0.08 | 1.42 | 0.38 | 0.65 | 2.66 | 0.17 |
| 11.901 | 0.14 | 0.08 | 1.62 | 0.42 | 0.65 | 2.87 | 0.18 |

**Table 3.** Critical velocities with corresponding heat release rates (default settings, $\chi_r$ obtained from simulations).

| $Q$ (kW) | $v_{cr}$ experiments [1] (m/s) | $v_{cr}$ FDS simulations (m/s) | radiative fraction $\chi_r$ (%) |
|---|---|---|---|
| 1.5 | 0.34 | 0.38 | 37 |
| 3.0 | 0.40 | 0.47 | 39 |
| 7.5 | 0.50 | 0.61 | 43 |
| 10.5 | 0.54 | 0.67 | 44 |
| 12.0 | 0.56 | 0.68 | 45 |
| 15.0 | 0.59 | 0.70 | 46 |
| 22.5 | 0.65 | 0.75 | 48 |

**Table 4.** Critical velocities with corresponding heat release rates (adiabatic simulations, $\chi_r = 0.43$ assumed for calculation of $Q$).

| $Q_{conv}$ | $Q$ | $v_{cr}$ |
|:---:|:---:|:---:|
| (kW) | (kW) | (m/s) |
| 1.0 | 1.7 | 0.37 |
| 2.0 | 3.4 | 0.46 |
| 4.9 | 8.6 | 0.62 |
| 6.8 | 12.0 | 0.67 |
| 7.8 | 13.7 | 0.67 |
| 9.8 | 17.1 | 0.70 |
| 14.6 | 26.7 | 0.73 |

**Table 5.** Maximum temperatures near the ceiling found in the numerical simulations.

| $Q$ | (kW) | 1.5 | 3.0 | 7.5 | 10.5 | 12.0 | 15.0 | 22.5 |
|---|---|---|---|---|---|---|---|---|
| $T_{max}$ | (K) | 381 | 420 | 615 | 803 | 864 | 923 | 1136 |
| $\int_{A_c}(T-373)\,dA$ | (m$^2$K) | 0 | 0 | 54 | 93 | 147 | 215 | 387 |
| $Q_{loss}$ | (kW) | | | 0.5 – 0.8 | 0.9 – 1.4 | 1.5 – 2.2 | 2.2 – 3.2 | 3.9 – 5.8 |